Astron. Astrophys. 327, 317–324 (1997)

ASTRONOMY
AND
ASTROPHYSICS

Photoevaporation of protostellar disks

II. The importance of UV dust properties and ionizing flux

Sabine Richling and Harold W. Yorke

Astronomisches Institut der Universität Würzburg, Am Hubland, D-97074 Würzburg, Germany
(email: richling@astro.uni-wuerzburg.de, yorke@astro.uni-wuerzburg.de)

Received 13 March 1997 / Accepted 27 May 1997

Abstract. We study the hydrodynamic evolution of protostellar disks under the influence of a central source of ionizing radiation and its stellar wind. Here we examine the effects of an important contribution to the diffuse radiation field – the scattering of hydrogen-ionizing photons on dust grains (dust scattering). We present and discuss the resulting changes in the evolution of the system under a variety of conditions both with and without dust scattering. An important consequence is the significant increase in the photoevaporation rate. Depending on the scattering coefficient assumed, the presence of dust within the ionized region can increase the density and flow of ionized material and correspondingly shorten the disk's lifetime by a factor of two or more. In addition, the temperature of the ionized outflowing gas is slightly higher and remains more nearly constant over the extent of the ionized region, even in the regions shadowed from direct stellar radiation.

We also investigate the influence of other major parameters of the problem, wind velocity, wind mass loss rate, and stellar ionizing flux, by systematically varying these parameters. Over a large range of values of stellar ionizing flux $S_{\rm star}$ we find a power law dependence of the disk mass loss rate due to photoionization $\dot{M}_{\rm ph} \propto S_{\rm star}^{0.58}$ which is comparable to analytic estimates. Deviations from this power law occurred for moderate values $S_{\rm star} \gtrsim 10^{47}$ s^{-1} due to our finite disk size and for low values $S_{\rm star} \lesssim 10^{45}$ s^{-1} due to the resulting non-steady flow pattern. Because we have assumed a warm ($T \approx 10^4$ K) wind and have included heating, cooling, ionization, and recombination processes in the stellar wind, we find that the disk's photoevaporation rate depends on the assumed wind parameters in a manner which can be explained by the loss of UV ionizing photons very close to the central star.

Key words: radiation transfer – stars: circumstellar matter – stars: formation of – ISM: jets and outflows – HII regions

Send offprint requests to: S. Richling

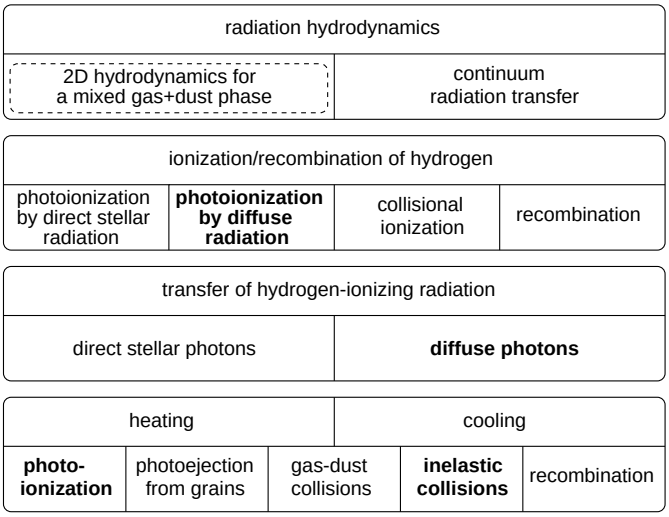

Fig. 1. Components of the 2D radiation hydrodynamics code. For more details see Paper I. Bold printed parts have been modified when including dust scattering.

1. Introduction

Circumstellar disks are a common byproduct of the star formation process. Their existence even in the harsh environment of the Orion Trapezium region has been confirmed by direct HST imaging (e.g. O'Dell et al. 1993; McCaughrean & O'Dell 1996). Those disks close to the O7 star Θ^1 Ori C are subject to photoevaporation and interaction with the O star's wind. Their HST images display arc-like morphologies with photoionized cusps being aligned toward Θ^1 Ori C. Because massive stars generally do not form in isolation, it is safe to assume that their winds and hydrogen-ionizing radiation will often interact with young protostellar disks – either one surrounding the ionizing source itself or those around close companions or those in the general vicinity. Indeed, the photoionization of an OB star's circumstellar disk is a viable model for many of the ultracompact HII regions (UCHIIs) in the lists of Wood & Churchwell (1989a,b), as suggested independently by Hollenbach et al. (1993) and

Table 1. Scattering coefficient $\kappa_{\rm dust}^{\rm scat}/\rho$ as well as parameters for the stellar wind (mass loss rate $\dot{M}_{\rm wind}$ and velocity $v_{\rm wind}$) and the ionizing source (stellar photon rate $S_{\rm star}$ and temperature $T_{\rm eff}$) used in the calculations. The photoevaporation rate $\dot{M}_{\rm ph}$ is determined as described in the text. The evaporation time scale $t_{\rm evap}$ is calculated from $t_{\rm evap} = M_{\rm disk}/\dot{M}_{\rm ph}$ with $M_{\rm disk} = 1.67\,{\rm M}_\odot$.

case	$\kappa_{\rm dust}^{\rm scat}/\rho$ $\rm cm^2 g^{-1}$	$\dot{M}_{\rm wind}$ $10^{-8}{\rm M}_\odot{\rm yr}^{-1}$	$v_{\rm wind}$ $\rm km\,s^{-1}$	$\log_{10} S_{\rm star}$ $\rm s^{-1}$	$T_{\rm eff}$ K	$\dot{M}_{\rm ph}$ $10^{-6}{\rm M}_\odot{\rm yr}^{-1}$	$t_{\rm evap}$ 10^6 yr
A	0	2	50	46.89	30 000	0.565	2.96
B	100	2	50	46.89	30 000	0.978	1.71
C	200	2	50	46.89	30 000	1.35	1.24
D1	0	2	50	44.91	15 000	0.014	118
D2	0	2	50	45.29	16 000	0.067	24.9
D3	0	2	50	45.67	17 500	0.120	13.9
D4	0	2	50	46.10	20 000	0.226	7.40
D5	0	2	50	46.46	23 000	0.333	5.02
D6	0	2	50	47.47	30 000	0.861	1.94
E1	200	2	50	45.67	17 500	0.263	6.34
E2	200	2	50	46.10	20 000	0.482	3.47
E3	200	2	50	46.46	23 000	0.776	2.15
E4	200	2	50	47.47	30 000	2.19	0.765
E5	200	2	50	48.07	30 000	3.29	0.507
F1	200	0.02	50	46.89	30 000	1.49	1.12
F2	200	0.2	50	46.89	30 000	1.46	1.15
F3	200	20	50	46.89	30 000	1.04	1.60
F4	200	200	50	46.89	30 000	—	—
G1	200	2	200	46.89	30 000	1.53	1.09
G2	200	2	400	46.89	30 000	1.65	1.01
G3	200	2	600	46.89	30 000	1.67	1.00
G4	200	2	1000	46.89	30 000	1.64	1.02

Yorke (1993) and calculated semi-analytically by Hollenbach et al. (1994, hereafter HJLS) and numerically by Yorke & Welz (1993; 1996, the latter will hereafter be referred to as Paper I).

The fact that many of the UCHIIs in the original lists of Wood & Churchwell are "cometary" in appearance (see also the supplements to this list by Kurtz et al. 1994) has led to the proposal by Van Buren et al. (1990) and Mac Low et al. (1991) that bow shocks from O stars moving through dense molecular clumps are responsible for many of the UCHIIs. However, the long path lengths of high density material and the high velocities required by this model make it unlikely that a significant fraction of UCHIIs can be explained by this mechanism.

In this series of papers we wish to test the hypothesis that most UCHIIs – even the irregular and cometary types – can be explained by the interaction of circumstellar disks with stellar winds and hydrogen-ionizing radiation. We will not restrict ourselves to the highly symmetrical cases considered in Paper I and HJLS: i.e. a disk surrounding a central source isolated and at rest with respect to a uniform ambient medium. Instead, we shall consider a variety of configurations: a star and its disk moving relative to both uniform and non-uniform media and cases whereby an O star does not have a disk of its own but one or more of its close companions in a multiple system do. In these cases we can expect highly complex flows to result. In order to follow this flow a robust numerical radiation hydrodynamics code is required.

The necessary improvements to the code of Paper I are discussed here as well as our first results. In Sect. 2 we discuss the numerical model in detail and in Sect. 3 we present the results of numerical radiation hydrodynamic calculations of several specific cases. In particular, we are interested in the effects of dust scattering. A summary of the results and our conclusions are given in Sect. 4.

2. Dust scattering

The physical processes taken into consideration are summarized in Fig. 1. The boxes and sub-boxes represent the components of our 2D radiation hydrodynamics code. Most of the physical model and numerical methods used are already described in detail in Paper I and Yorke & Kaisig (1995). Here we concentrate on the extensions or modifications made in order to include the diffuse radiation field resulting from hydrogen-ionizing photons scattered on dust grains. Several parts of the code (bold printed in Fig. 1) are affected by this procedure.

To simplify the photoionization model we consider ionization of hydrogen only. When calculating the degree of ionization x in a scattering medium, additional effects due to the scattered photons must be taken into account. The time dependent rate equation is now given by

$$\frac{\partial \rho x}{\partial t} + \nabla \cdot (\rho x \mathbf{v}) =$$

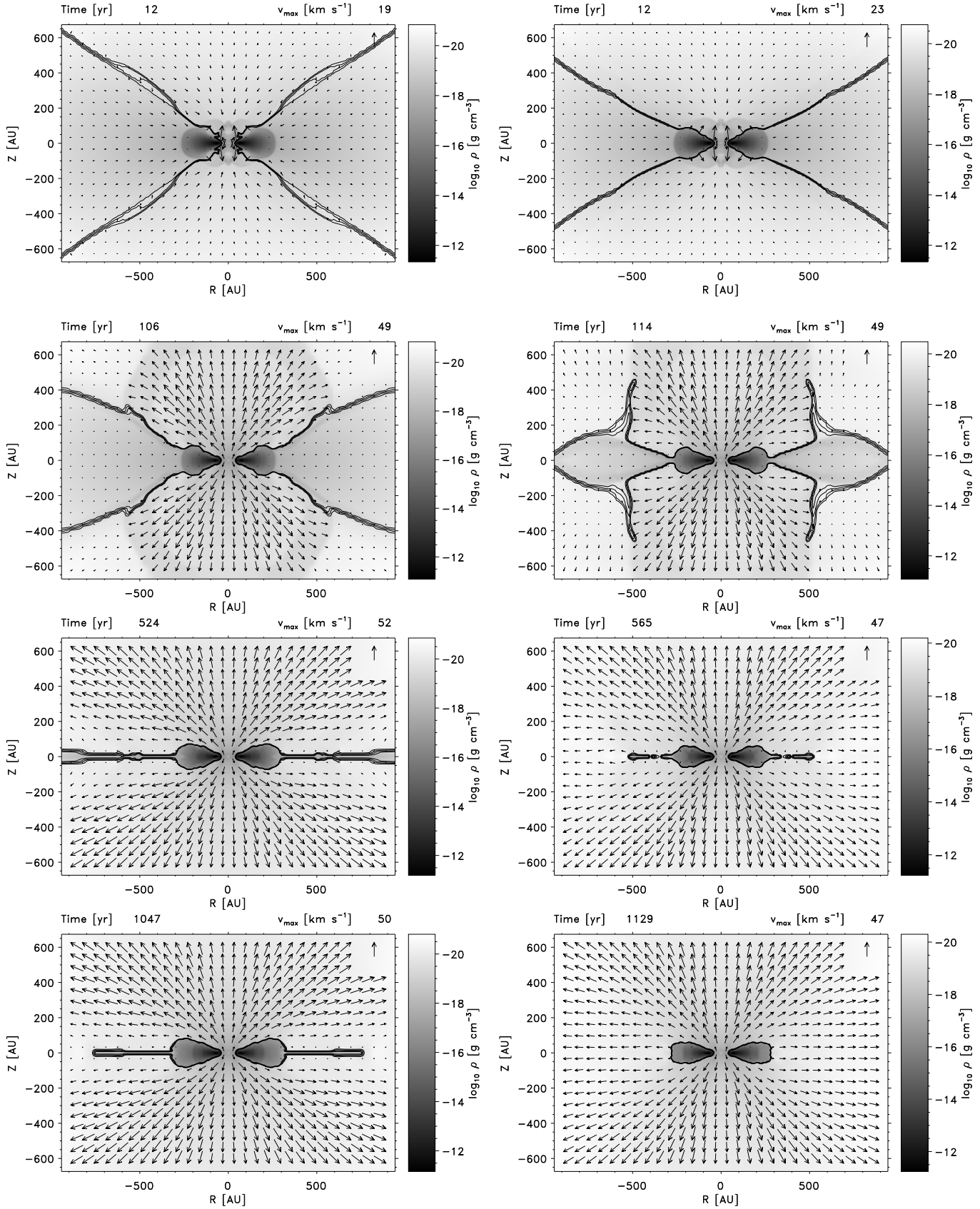

Fig. 2. Early evolution of the star-disk system after the onset of the hydrogen-ionizing radiation and a very weak stellar wind ($\dot{M}_{\rm wind} = 2 \times 10^{-8}\,{\rm M}_\odot{\rm yr}^{-1}$, $v_{\rm wind} = 50\,{\rm km\,s}^{-1}$). The frames on the left(right) refer to the simulation without(with) dust scattering (cases A and C in Table 1). The gray scale depicts the density structure, the arrows the velocity field, normalized to the maximum velocity. The black lines are contours of constant degree of ionization and given for $x = 0.2,\ 0.4,\ 0.6$ and 0.8.

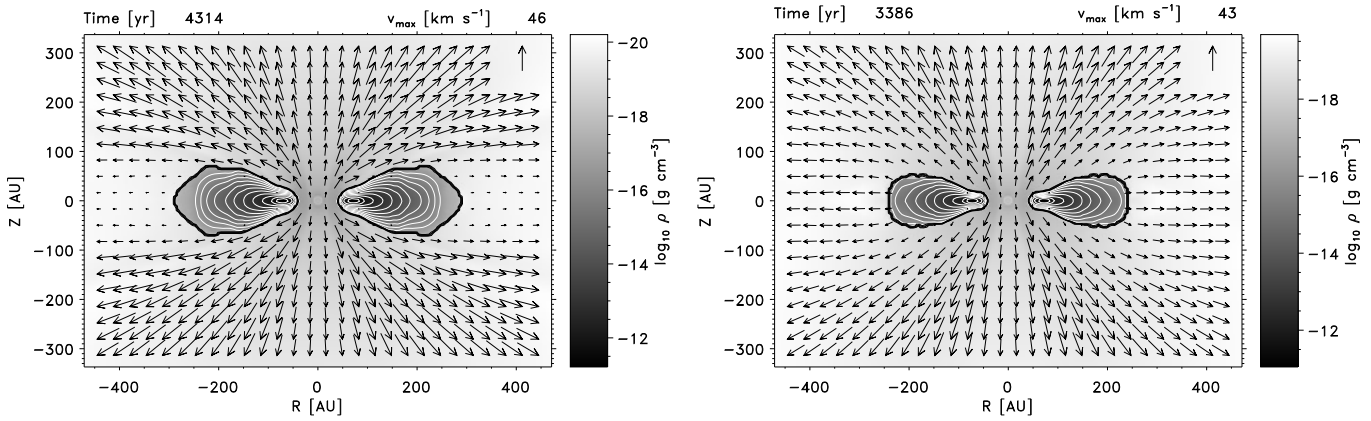

Fig. 3. Final quasi-steady states of the simulations in Fig. 2. Again, the picture on the left(right) refers to the simulation without(with) dust scattering. In addition, white contour lines are given for the density within the disk which vary from $\log \rho = -11.5$ to $\log \rho = -16.5$ in increments of $\Delta \log \rho = 0.5$.

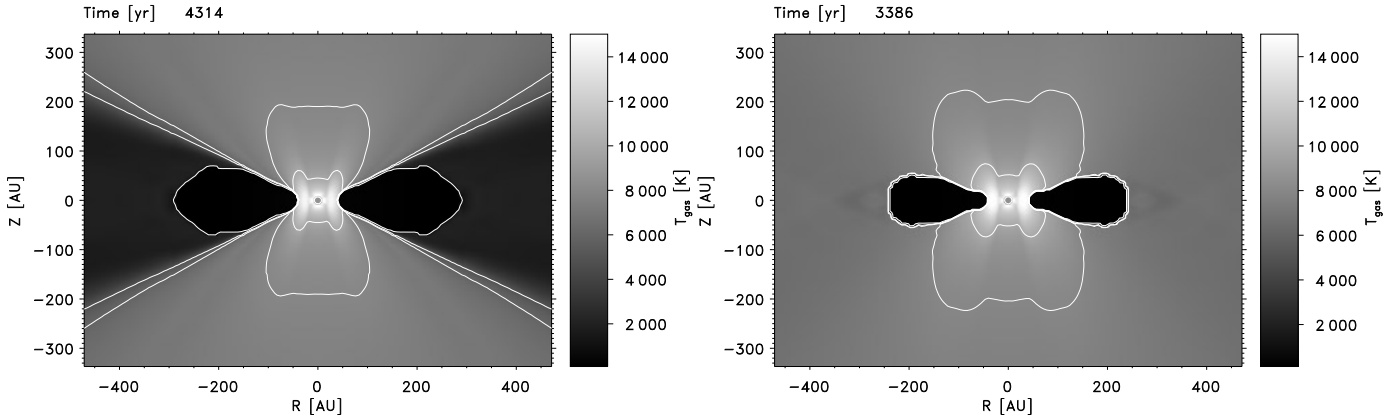

Fig. 4. Temperature of the gas for the quasi-steady states shown in Fig. 3. The white contour lines correspond to $T_{\rm gas}$ = 1 000, 5 000, 6 000, 8 000 and 10 000 K. Note the sharp temperature decrease at the edge of the disk.

$$\rho(1-x)[\sigma_{\rm star}u_{\rm star} + \sigma_{\rm rec}u_{\rm rec} + \sigma_{\rm star}u_{\rm dust}]c \qquad (1)$$
$$+\rho C(T_{\rm gas})nx(1-x) - \rho\alpha(T_{\rm gas})nx^2 \quad ,$$

where ρ and $\mathbf{v}$ are the density and the velocity of the gas. The terms on the right hand side of the equation containing the photon densities $u_{\rm star}$, $u_{\rm rec}$ and $u_{\rm dust}$ refer to the contributions to the ionization by direct stellar photons, by photons originating from recombinations of hydrogen directly into the ground state and by scattered photons, respectively. Because we assume the scattering coefficient $\kappa^{\rm scat}_{\rm dust}$ to be frequency independent, the scattering process does not change the spectral shape of the photon density distribution and the same mean ionization cross section of hydrogen $\sigma_{\rm star}$ can be used for scattered photons as for direct stellar photons. The remaining terms are the contributions from collisional ionization and from recombination, where $C(T_{\rm gas})$, $\alpha(T_{\rm gas})$, and n are the collisional ionization coefficient, the total recombination coefficient and the particle density.

The photon density of scattered photons $u_{\rm dust}$ is calculated in the same way as the photon density of recombination photons $u_{\rm rec}$: we use the flux-limited diffusion (FLD) approximation (Levermore & Pomraning 1981, Yorke & Kaisig 1995) for the relation between the photon flux density $\mathbf{F}$ and the photon density u

$$\mathbf{F} = -\frac{\lambda c}{\chi^{\rm ext}}\nabla u \quad , \qquad (2)$$

where the flux-limiter λ is defined as

$$\lambda = \frac{1}{S}\left(\coth S - \frac{1}{S}\right) \quad \text{with} \quad S = \frac{|\nabla u|}{\chi^{\rm ext}u} \quad . \qquad (3)$$

We finally solve

$$\frac{\partial u_{\rm dust}}{\partial t} - \nabla\cdot\left(\frac{\lambda c}{\chi^{\rm ext}_{\rm dust}}\nabla u_{\rm dust}\right) = \epsilon - \chi^{\rm abs}_{\rm dust}cu_{\rm dust} \quad , \qquad (4)$$

where the source term ϵ for photons scattered on dust grains is calculated from

$$\epsilon = \kappa^{\rm scat}_{\rm dust}cu_{\rm star} \quad . \qquad (5)$$

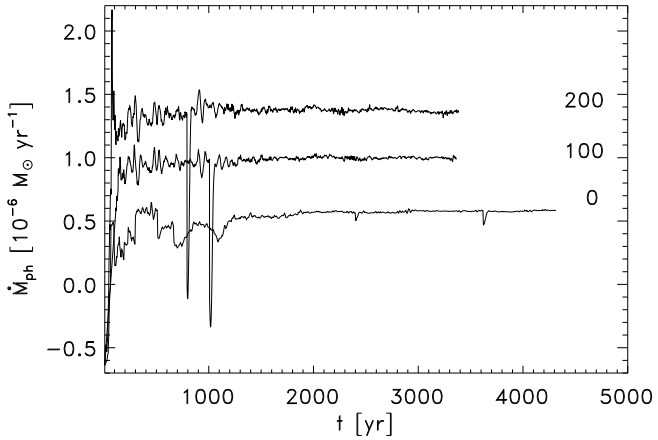

Fig. 5. Time evolution of the photoevaporation rate for different values of $\kappa^{\rm scat}_{\rm dust}/\rho\,[{\rm cm^2\,g^{-1}}]$ (cases A, B and C in Table 1).

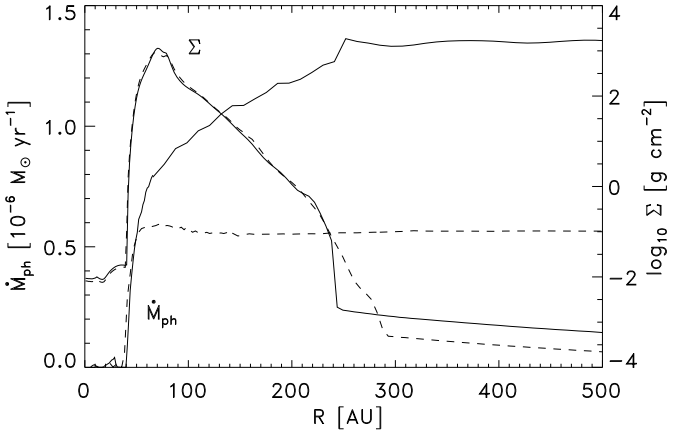

Fig. 6. Surface density Σ and photoevaporation rate $\dot{M}_{\rm ph}$ as a function of radius for the quasi-steady states of case A (dashed lines) and C (solid lines).

The extinction and absorption coefficients include the contributions from both gas and dust

$$\chi^{\rm ext}_{\rm dust} = n(1-x)\sigma_{\rm star} + \kappa^{\rm ext}_{\rm dust} \quad ,$$
$$\chi^{\rm abs}_{\rm dust} = n(1-x)\sigma_{\rm star} + \kappa^{\rm abs}_{\rm dust} \quad . \qquad (6)$$

With the grain size distribution of Mathis et al. (1977) $n(a) \propto a^{-3.5}$ for $0.005\,\mu{\rm m} \le a \le 0.25\,\mu{\rm m}$ many of the grains are larger than the wavelength of Lyman continuum photons ($\lambda \le 0.091\,\mu$m). Thus, a relatively high value for the isotropic scattering coefficient per gram gas $\kappa^{\rm scat}_{\rm dust}/\rho$ can be expected. In our calculations we generally use $\kappa^{\rm scat}_{\rm dust}/\rho = 200\,{\rm cm^2\,g^{-1}}$, but cases are calculated with both smaller and larger values for comparison purposes. Sublimation of dust grains takes place only close to the central star where the dust temperature exceeds approximately 1 000 K. Other mechanisms which may play a role in decreasing the number of very small particles are grain coagulation in the disk and sputtering in shocks (Dwek et al. 1996). The consequence would be a decrease in $\kappa^{\rm abs}_{\rm dust}/\rho$ (Laor & Draine 1993). In order to take these locally limited processes into account we adopt a moderate overall extinction coefficient $\kappa^{\rm ext}_{\rm dust}/\rho = 300\,{\rm cm^2\,g^{-1}}$. The contribution of Lyman continuum radiation to dust destruction should be unimportant since only grains with $a \le 0.001\,\mu$m are destroyed by X-rays (Voit 1991).

Lyman continuum photons scattered by dust grains also contribute to the energy balance:

$$\left(\frac{\partial e}{\partial t}\right)_{\rm dust} = n(1-x)\sigma_{\rm star} c u_{\rm dust}[\langle h\nu\rangle_{\rm star} - 13.6\,{\rm eV}] \quad , \qquad (7)$$

where $\langle h\nu\rangle_{\rm star}$ is the mean energy of the stellar photons with $h\nu > 13.6\,$eV. In contrast to the diffuse UV radiation field $u_{\rm rec}$ from hydrogen recombinations the component $u_{\rm dust}$ is able to ionize NI and OII. Hence, we can expect cooling due to forbidden line radiation of NII and OIII everywhere in the ionized regions.

He^+ and He^{++} recombination photons will also contribute to the UV diffuse background capable of ionizing NI and OII. We do not follow helium ionization explicitly, however. For the stellar temperatures considered here, $T_{\rm eff} \le 30\,000$ K, the flux of photons with $h\nu > 24.59$ eV is extremely small. For our purposes – estimating the source function for the diffuse UV background – the net effect of helium ionization by stellar photons followed by "on the spot" recombination is to convert radially moving stellar UV photons into nearly isotropic components within the HeII and HeIII ionization zones. In principle this effect can be roughly included by appropriately modifying our dust parameters. In practice, however, our ignorance of both the stellar UV flux and the true dust properties in this regime makes such an exercise a purely academic one.

As in Paper I we begin our calculations with a star-disk model resulting from a collapse simulation of a $10\,M_\odot$ rotating cloud (Yorke et al. 1995): a $8.4\,M_\odot$ star surrounded by a $1.67\,M_\odot$ disk. Then we calculate the further evolution of the system under the influence of hydrogen-ionizing radiation and a stellar wind.

3. Results

A summary of the cases calculated, the parameters assumed, and some of the results is given in Table 1. First, we performed two simulations to investigate the effects of the additional diffuse radiation field. Fig. 2 shows the early evolution of the system, i.e. the density and velocity structure at four evolutionary times. The frames to the left(right) refer to the simulation without(with) dust scattering. The simulation without dust scattering corresponds to "case P" discussed in detail in Paper I. The black contour lines mark the position of the ionization front which separates the hot ionized gas from the cool neutral material. The overall evolution of each simulation is similar. However, dust scattering allows an increased number of ionizing photons to reach the "shadow" of the disk. Furthermore, these photons tend to be "harder" (more energetic) than the diffuse photons from recombinations directly into the ground state. As a result, the cone of ionized gas opens somewhat faster and the compressed

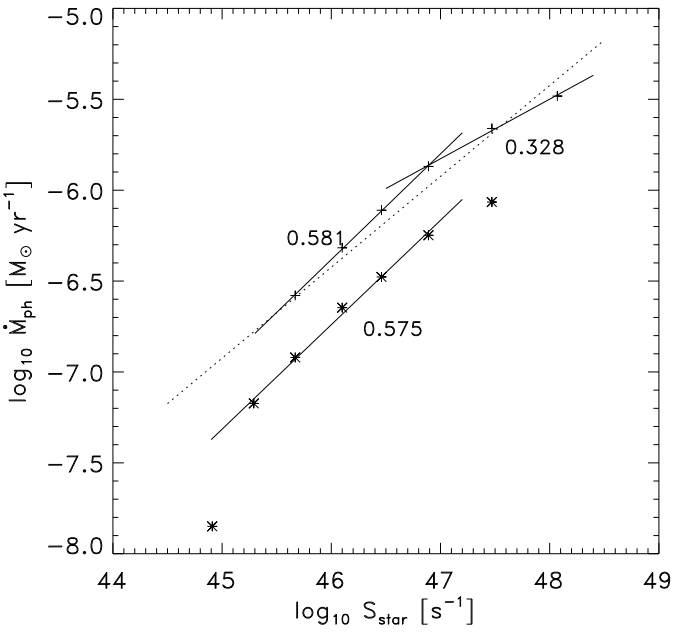

Fig. 7. Dependence of the photoevaporation rate $\dot{M}_{\rm ph}$ on the stellar photon rate $S_{\rm star}$. The stars(crosses) are results from simulations without(with) dust scattering (cases A+D and C+E). Straight lines are the result of a power law fit; they are labeled with the appropriate power law index. The doted line is taken from HJLS.

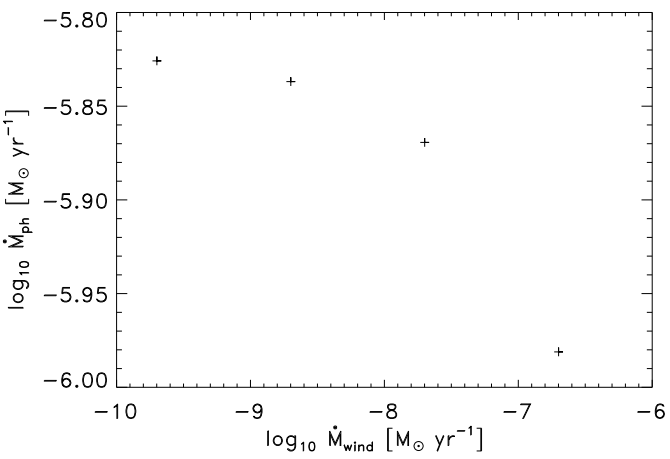

Fig. 8. Dependence of the photoevaporation rate $\dot{M}_{\rm ph}$ on the stellar mass loss rate $\dot{M}_{\rm wind}$ (cases C+F).

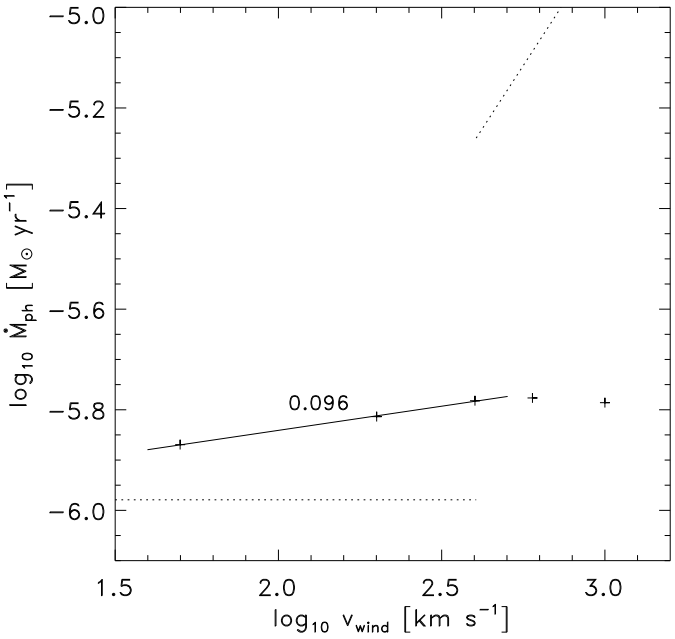

Fig. 9. Dependence of the photoevaporation rate $\dot{M}_{\rm ph}$ on the stellar wind velocity $v_{\rm wind}$ (cases C+G). The straight line is labeled by the exponent of a power law fit. The dotted lines refer to the "weak wind" and "strong wind" solutions of HJLS.

material in the equatorial plane behind the disk is completely ionized much earlier, when dust scattering is included.

The final quasi-steady state of the evolution is reached when the ionization front completely envelopes the densest parts of the disk (Fig. 3). Dust scattering leads to a disk which is more tightly compressed (i.e. its external pressure is higher). The velocity in the shadow regions close to the equatorial plane but beyond the disk is much higher than the comparison case without dust scattering. The temperature in the shadow regions (Fig. 4) differs significantly for the two cases. The heating by scattered photons is indeed more effective than the heating by recombinations photons alone.

In order to estimate the lifetime of the disk we measured the photoevaporation rate $\dot{M}_{\rm ph}$ by calculating the mass flowing through a cylinder enclosing the entire disk and subtracting the mass loss rate of the star. In Fig. 5 the evolution of $\dot{M}_{\rm ph}$ is shown for different values of $\kappa_{\rm dust}^{\rm scat}/\rho$. The photoevaporation rate of the simulation which includes the effect of dust scattering and assumes a value $\kappa_{\rm dust}^{\rm scat}/\rho$ = 200 cm^2 g^{-1} is more than twice as high as the one without.

Fig. 6 shows which parts of the disk are responsible for the increase in the photoevaporation rate. Here $\dot{M}_{\rm ph}(r)$ through a cylinder of radius r and height $2r$ is plotted together with the surface density $\Sigma(r) = \int \rho\, dz$. For case A (without dust scattering: dashed lines) $\dot{M}_{\rm ph}$ originates mainly from the inner edge of the disk, whereas for case C (with dust scattering: solid lines) we find a non-negligible contribution to $\dot{M}_{\rm ph}$ over the entire surface of the disk.

We have performed several additional calculations to test the influence of the stellar UV-photon rate $S_{\rm star}$, the wind velocity $v_{\rm wind}$, and the stellar mass loss rate $\dot{M}_{\rm wind}$, whereby these parameters are varied systematically.

In Fig. 7 the dependence of $\dot{M}_{\rm ph}$ on $S_{\rm star}$ is shown. The different plotting symbols refer to the results without ($*$) and with (+) UV dust scattering. We gained each value for $\dot{M}_{\rm ph}$ by starting from the quasi-steady states shown in Fig. 3, changing $S_{\rm star}$, and then continuing the calculations until a new quasi-steady state has been attained. In order to compare our results with the semi-analytical, infinitely thin disk models of HJLS, we fit a power law to the $\dot{M}_{\rm ph}$ distributions when possible. For median values

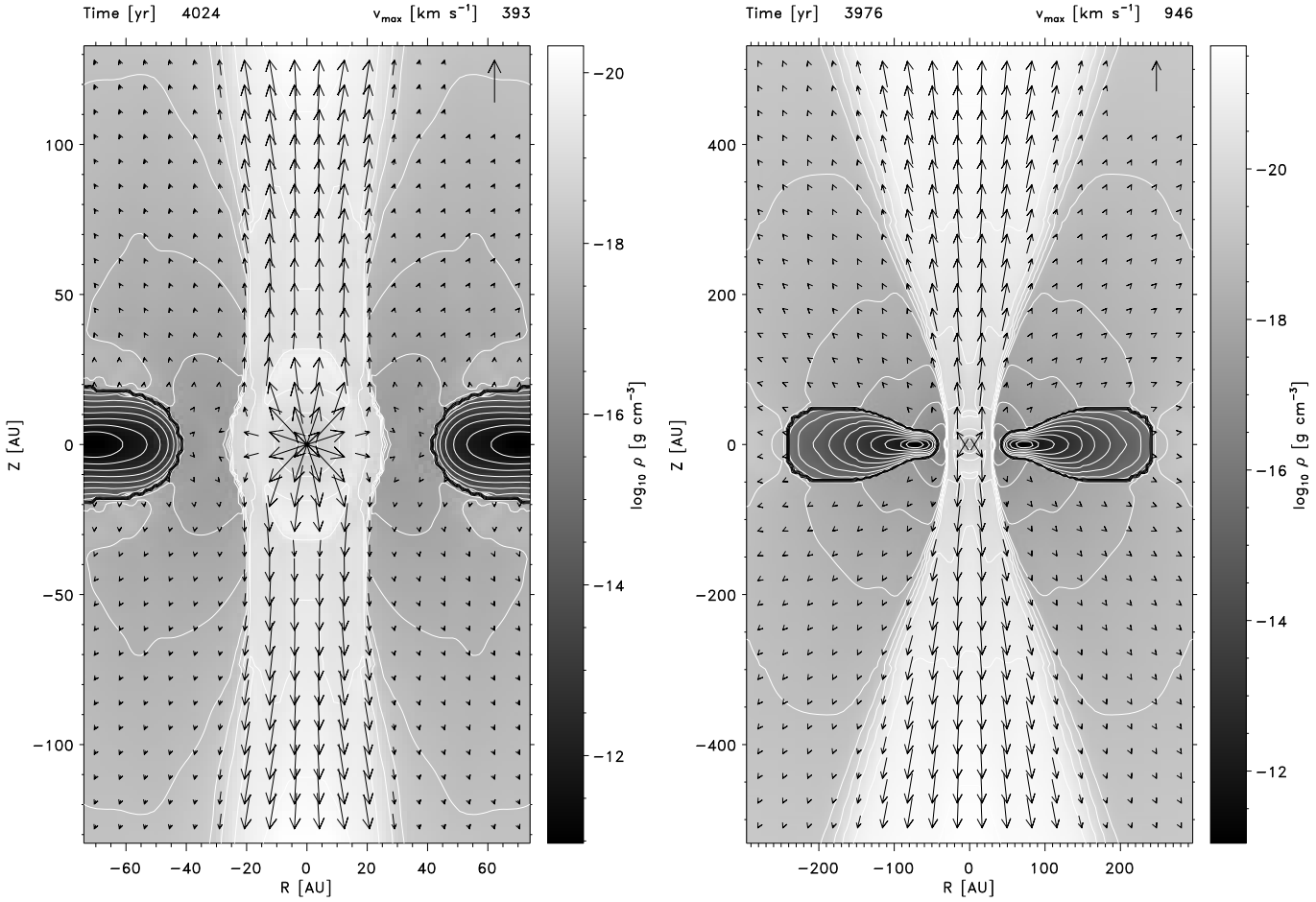

Fig. 10. Density, velocity and ionization structure for simulations with stellar wind velocities of 400 and 1 000 km s^{-1} (cases G2 and G4). Here the white contour lines for the density vary from $\log \rho = -11.5$ to $\log \rho = -21.5$ in increments of $\Delta \log \rho = 0.5$.

of $S_{\rm star}$ between 10^{45} s^{-1} and 10^{47} s^{-1} we obtain a power law exponent $\alpha \approx 0.58$ for the simulations both with and without dust scattering. This result is in reasonably good agreement with the weak wind solution of HJLS, who deduced an exponent of $\alpha = 0.5$ (dotted line in Fig. 7). Note that numerical values for $\dot{M}_{\rm ph}(S_{\rm star})$ from HJLS are comparable with our solutions.

The mass loss rate resulting from the lowest value for $S_{\rm star}$ could not be included in the power law expression, because only part of the disk's immediate environment could be kept ionized. Additional neutral regions appeared in the flow and no quasi-steady state was attained. For values of $S_{\rm star}$ exceeding 10^{47} s^{-1} we obtained a power law exponent $\alpha \approx 0.3$, falling well below HJLS's predicted value. We attribute this to the finite radial extension of our disk, whereas HJLS assumed an infinitely thin disk which extended out to infinity.

In Fig. 8 we show how $\dot{M}_{\rm ph}$ decreases with increasing $\dot{M}_{\rm wind}$. This effect can be attributed to the high gas densities in a stellar wind close to the central source. For a given wind velocity $v_{\rm wind}$ and stellar mass loss rate $\dot{M}_{\rm wind}$, the density is given by

$$\rho_{\rm wind}(r) = \frac{\dot{M}_{\rm wind}}{4\pi r^2 v_{\rm wind}} \quad . \tag{8}$$

Because the recombination rate per unit volume increases as ρ^2, an increased value for $\dot{M}_{\rm wind}$ leads to increased fraction of stellar UV photons which become absorbed in the immediate vicinity of the star. In extreme cases this can lead to complete "squelching" of an HII region (e.g. Yorke 1986), a phenomenon evident in our calculation with $\dot{M}_{\rm wind} = 2 \times 10^{-6}\,{\rm M}_\odot{\rm yr}^{-1}$ (case F4), where no UV photons are able to leave the central "wind generator" region.

Finally, we investigated the dependence of $\dot{M}_{\rm ph}$ on $v_{\rm wind}$. In Fig. 9 the results are plotted together with the power law solution of HJLS, who distinguish between two extreme regimes. The transition between a "weak wind" and a "strong wind" occurs when the ram pressure of the wind is equal to the thermal pressure of the photoevaporating flow. For the weak wind case we get a weak dependence on $v_{\rm wind}$ which is comparable to the solution of HJLS. But we cannot reproduce the strong increase in $\dot{M}_{\rm ph}$ for the strong wind regime. This is probably due to the fact that on the one hand our disk is not infinitely thin but has some vertical extension and a toroidal shape. Thus, our initially spherical symmetric wind becomes hydrodynamically focussed along the rotational axis and the effective wind pressure at the disk's surface is significantly reduced. This effect

can be seen for example in Fig. 10 which shows the density and velocity structure of the system for $v_{\rm wind} = 400\,{\rm km\,s^{-1}}$ and $v_{\rm wind} = 1\,000\,{\rm km\,s^{-1}}$.

On the other hand, we included the effects of heating, cooling, ionization and recombination in the wind material. The equilibrium temperature in the freely expanding (unshocked) part of the wind (see schematic structure discussed in Paper I, especially Figs. 11 and 12) attained values of $T \approx 10^4$ K. Thus, some of the available stellar UV photons were absorbed in the wind itself. It is conceivable that a hot ($T \gtrsim 10^6$ K) stellar wind will remain collisionally ionized and thus transparent to the stellar UV photons and a more efficient photoionization of the disk will result.

Fig. 10 shows that we are able to produce strongly collimated outflows without invoking magnetic fields. Such bipolar structures are a frequently observed phenomenon in the case of low mass star formation. But there are also observational indications of bipolar molecular and/or ionized outflows (e.g. Gaume et al. 1995; Shepherd & Churchwell 1996a,b; Deharveng et al. 1997) in regions of massive star formation associated with UCHIIs. Observations of rotation in the ionized gas point to an involvement of circumstellar disks in the formation process of these outflows (De Pree et al. 1995).

Our calculated disk destruction time scales are of order 10^6 yr for our $1.67\,{\rm M}_\odot$ disk (see Table 1). Dust scattering has a significant effect, but the most decisive parameter turns out to be the stellar photon rate.

4. Summary

We have presented a versatile, robust code for following the evolution of circumstellar disks under the influence of hydrogen-ionizing radiation and strong stellar winds. We have used this code to investigate the relative importance of the key parameters of the problem of an OB star interacting with its own disk. Our main results are summarized in Table 1 and discussed in detail in the previous section. The resulting quasi-steady ionized flows would be interpreted as ultracompact HII regions. Because of the symmetry assumed for this first set of cases, solutions which are both axially symmetric and symmetric with respect to the equatorial plane were found.

Although UCHIIs which appear to have a high degree of symmetry are found in the lists of Wood & Churchwell (1989a,b), most observed UCHIIs display either a prominent asymmetry (e.g. cometary-type UCHIIs) or are highly irregular. We contend that these UCHIIs could also be explained by the photoionization of disks in a more complex environment. O stars often have close companions, some of which may have disks. The interaction of multiple photoevaporation flows with each other and with (possibly multiple) stellar winds in a non-uniform, non-stationary external medium will certainly be able to break up the symmetry of our idealized boundary conditions and initial configurations. This will be a subject of later investigations in this series.

Acknowledgements. We thank David Hollenbach for interesting discussions and useful comments. This research has been supported by the Deutsche Forschungsgemeinschaft (DFG) under grant number Yo 5/19-1. The calculations were performed at the HLRZ in Jülich and the LRZ in Munich.

References

Deharveng L., Zavagno A., Cruz-González I., Salas L., Caplan J., Carrasco L. 1997, A&A, 317, 459.
De Pree C.G., Rodríguez L.F., Dickel H.R., Goss W.M., 1995 ApJ, 447, 220.
Dwek E., Foster S.M., Vancura O. 1996, ApJ, 457, 244.
Gaume R.A., Goss W.M., Dickel H.R., Wilson T.L., Johnston K.J. 1995, ApJ, 438, 776.
Hollenbach D., Johnstone D., Shu F. 1993, ASP Conf. Ser. 35, 26.
Hollenbach D., Johnstone D., Lizano S., Shu F. 1994, ApJ, 428, 654 (HJLS).
Kurtz S., Churchwell E., Wood D.O.S. 1994, ApJS, 91, 659.
Laor A., Draine B.T. 1993, ApJ, 402, 441.
Levermore C., Pomraning G. 1981, ApJ, 248, 321.
Mac Low M.-M., Van Buren D., Wood D.O.S., Churchwell E. 1991, ApJ, 369, 395.
Mathis J.S., Rumpl W., Nordsieck K.H. 1977, ApJ, 215, 425.
McCaughrean M.J., O'Dell C.R. 1996, AJ, 111, 1977.
O'Dell C.R., Wen Z., Hu X. 1993, ApJ, 410, 696.
Shepherd D.S., Churchwell E. 1996a, ApJ, 457, 267.
Shepherd D.S., Churchwell E. 1996b, ApJ, 472, 225.
Van Buren D., Mac Low M.-M., Wood D.O.S., Churchwell E. 1990, ApJ, 353, 570.
Voit G.M. 1991, ApJ, 379, 122.
Wood D.O.S., Churchwell E. 1989a, ApJ, 340, 265.
Wood D.O.S., Churchwell E. 1989b, ApJS, 69, 831.
Yorke H.W. 1986, ARAA 24, 49.
Yorke H.W. 1993, ASP Conf. Ser. 35, 45.
Yorke H.W., Kaisig M. 1995, Comp. Phys. Comm., 89, 29.
Yorke H.W., Welz A. 1993, in *Star Formation, Galaxies and the Interstellar Medium*, eds. J. Franco, F. Ferrini, G. Tenorio-Tagle, (Cambridge Univ. Press), 239.
Yorke H.W., Welz A. 1996, A&A, 315, 555 (Paper I).
Yorke H.W., Bodenheimer P., Laughlin G. 1995, ApJ, 443, 199.

This article was processed by the author using Springer-Verlag LaTeX A&A style file *L-AA* version 3.